Supporting Information

Adjustable Anchoring of Ni/Co Cations by Oxygen-Containing Functional Groups on Functionalized Graphite Paper and Accelerated Mass/Electron Transfer for Overall Water Splitting

Yiyi Huang, [a] Lei Sun, [b] Zebin Yu, [*a] Ronghua Jiang, [c] Jun Huang, [d] Yanping Hou, [a] Fei Yang, [e] Boge Zhang, [a] Runzhi Zhang, [a] and Yalan Zhang [a]

a. School of Resources, Environment and Materials, Guangxi University, Nanning 530004, P. R. China.

b. School of Chemical Engineering and Technology, Hainan University, Haikou 570228, P. R. China.

c. School of Chemical and Environmental Engineering, Shaoguan University, Shaoguan 512005, P. R. China.

d. College of Civil Engineering and Architecture, Guangxi University, Nanning 530004, P. R. China.

e. Guangzhou Institution Energy Testing, Guangzhou 510170, P. R. China.

Corresponding author: Zebin Yu. Tel./fax.: + 8613877108420

E-mail: xxzx7514@hotmail.com (Z. Yu)

Figure of the content

Figure S1. XPS analysis of O 1s spectra: (a) $FGP_{0.48}$, (b) $FGP_{0.35}$, (c) $FGP_{0.44}$, and (d) $FGP_{0.41}$.

Figure S2. Raman spectra of $FGP_{0.48}$, $FGP_{0.35}$, $FGP_{0.44}$, and $FGP_{0.41}$ in the wavenumber region from 1000 to 3000 cm^{-1}.

Figure S3. FE-SEM images of $FGP_{0.48}$ (a and b), $FGP_{0.35}$ (c and d), $FGP_{0.44}$ (e and f), and $FGP_{0.41}$ (g and h).

Figure S4. CV curve of (a) $FGP_{0.48}$, (b) $FGP_{0.35}$, (c) $FGP_{0.44}$, and (d) $FGP_{0.41}$ under different scan rates.at a voltage range of 0.884 V-1.004 V (vs. RHE). (e) Plots of current density difference (Δj) at 0.944 V (vs. RHE) against different scan rates for calculation of C_{dl}.

Figure S5. (a) EIS plots of $FGP_{0.48}$, $FGP_{0.35}$, $FGP_{0.44}$, and $FGP_{0.41}$ at 0.924 V (vs. RHE). Inset: the enlarged EIS plots at the high-frequency region. (b) The resistivity comparison of $FGP_{0.48}$ and $FGP_{0.44}$.

Figure S6. Photoluminescence (PL) spectra for NCS-NCO/$FGP_{0.44}$.

Figure S7. CV curve of NCS-NCO/$FGP_{0.48}$ (a), NCS-NCO/$FGP_{0.35}$ (b), NCS-NCO/$FGP_{0.44}$ (c), NCS-NCO/$FGP_{0.41}$ (d), and NCO/$FGP_{0.44}$ (e) under different scan rates.

Figure S8. Raman spectra of NCS-NCO/$FGP_{0.48}$, NCS-NCO/$FGP_{0.35}$, NCS-NCO/$FGP_{0.44}$, and NCS-NCO/$FGP_{0.41}$ with their D and G peaks.

Figure S9. The comparison of C_{dl} from recent report carbon-based bifunctional electrocatalysts and NCS-NCO/$FGP_{0.44}$.

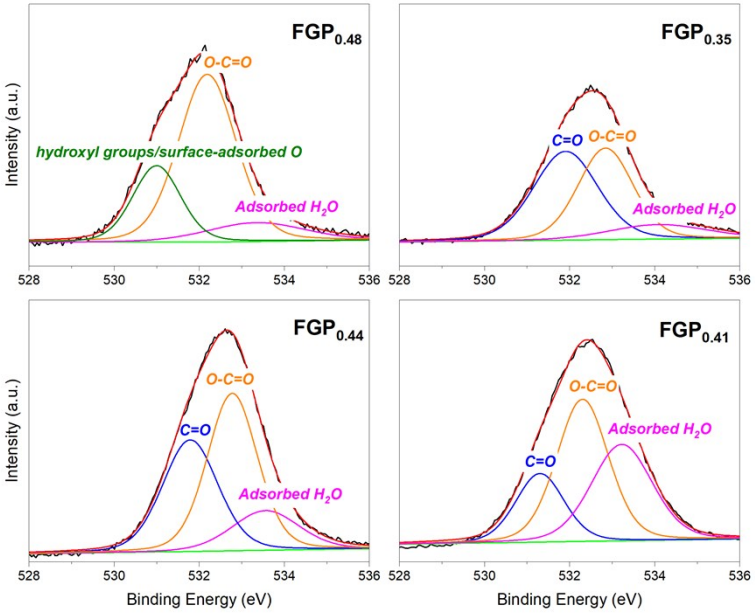

Figure S1. XPS analysis of O 1s spectra: (a) $FGP_{0.48}$, (b) $FGP_{0.35}$, (c) $FGP_{0.44}$, and (d) $FGP_{0.41}$.

The surface states of O species under different exfoliated times demonstrated in Fig. S1. Firstly, $FGP_{0.48}$ electrode corresponds to three peaks of hydroxyl groups/surface-adsorbed O (531.0 eV), O=C-O groups (532.2 eV), and absorbed H_2O (533.4 eV), respectively.[1-3] After electrochemical exfoliating, $FGP_{0.35}$, $FGP_{0.44}$, and $FGP_{0.41}$ electrodes correspond to three peaks of C=O (531.3-531.9 eV), O=C-O groups (532.3-532.8 eV), and absorbed H_2O (533.2-534.0 eV), respectively.[4] Obviously, this is consistent with the results of the XPS spectra of C 1s, which further confirms that the functionalized graphite paper electrode successfully introduced the oxygen-containing functional group.

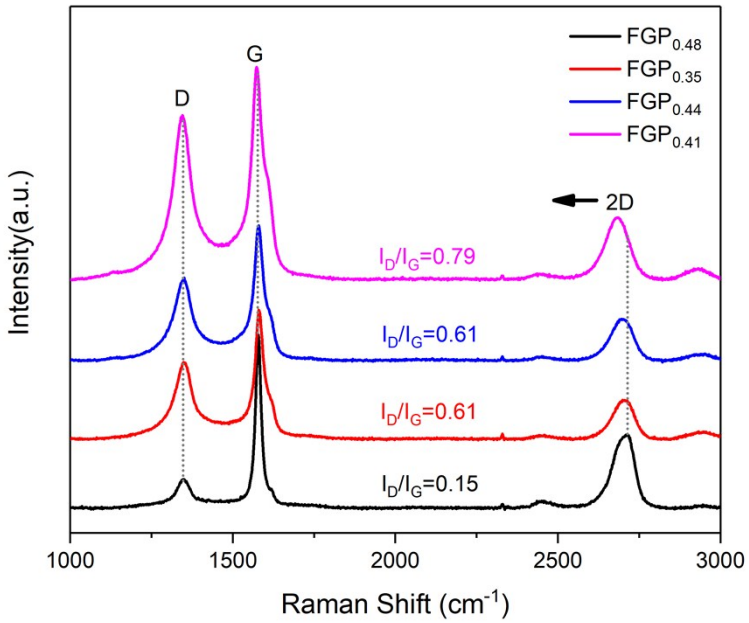

Figure S2. Raman spectra of $FGP_{0.48}$, $FGP_{0.35}$, $FGP_{0.44}$, and $FGP_{0.41}$ in the wavenumber region from 1000 to 3000 cm^{-1}.

To analyze the graphitization degree and defect degree of the graphite catalysts, the vibrational peaks of D-band, G-band, and 2D-band at ~1350, ~1580, and ~2670 cm^{-1} were measured. The D-band corresponds to the vibration of sp^3-hybridized carbon atoms in disordered and defective regions, while G-band belongs to the E_{2g} vibration mode of sp^2 carbon atom. Thus, using the I_D/I_G ratio can qualitatively evaluate the graphitization sequence and defects of carbonaceous materials. The 2D waveband is a two-phonon resonance mode, and its strength reflects the stacking degree of graphene.[5]

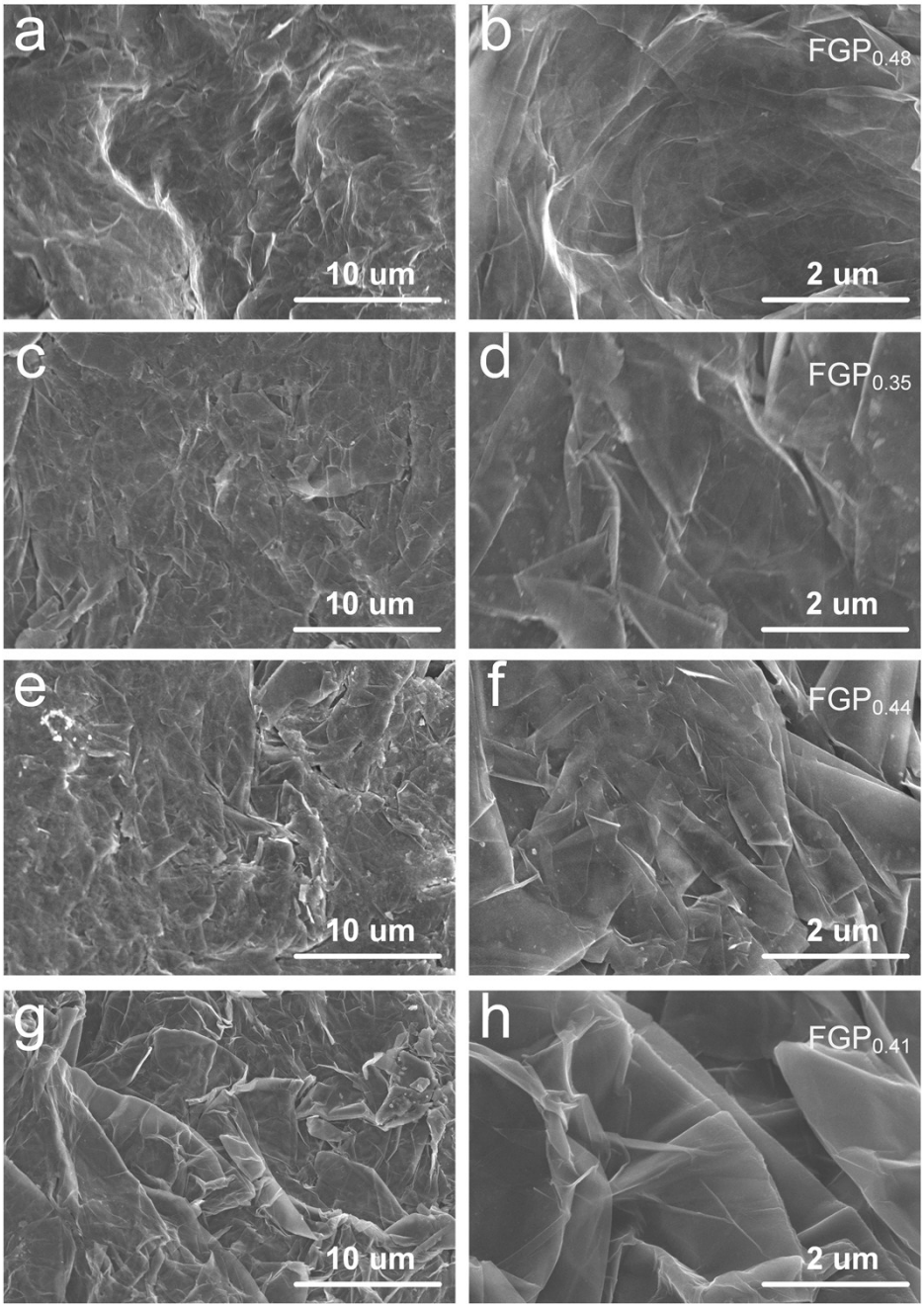

Figure S3. FE-SEM images of $FGP_{0.48}$ (a and b), $FGP_{0.35}$ (c and d), $FGP_{0.44}$ (e and f), and $FGP_{0.41}$ (g and h).

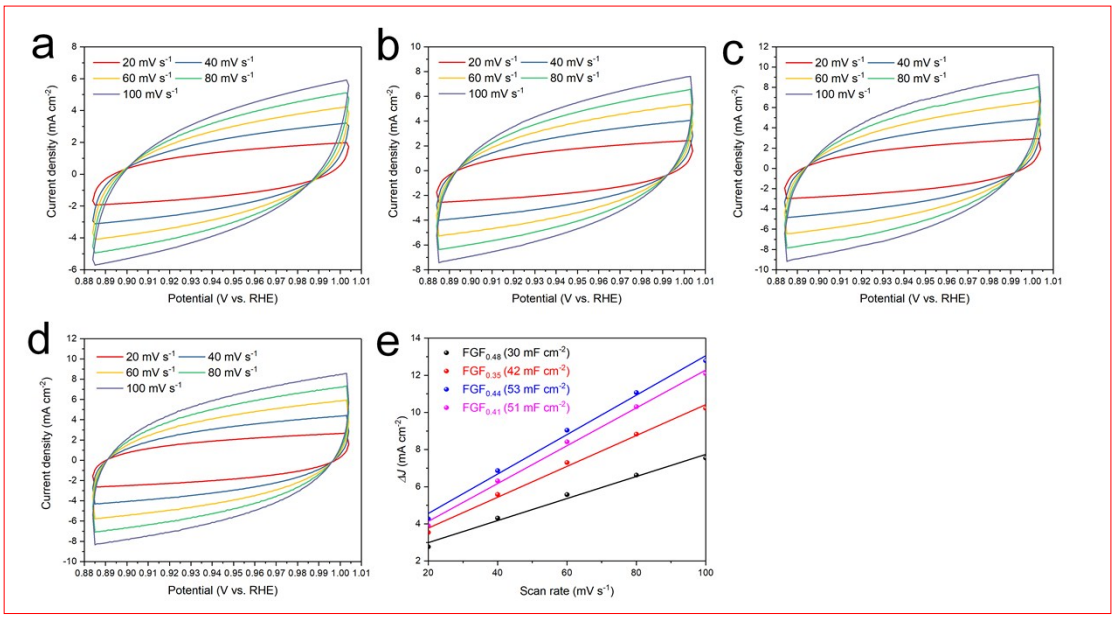

Figure S4. CV curve of (a) $FGP_{0.48}$, (b) $FGP_{0.35}$, (c) $FGP_{0.44}$, and (d) $FGP_{0.41}$ under different scan rates.at a voltage range of 0.884 V-1.004 V (vs. RHE). (e) Plots of current density difference (Δj) at 0.944 V (vs. RHE) against different scan rates for calculation of C_{dl}.

The C_{dl} of the FGP electrodes were calculated from the results of the CV scan, and the ECSA values were calculated (Figure S4a-e). The calculated C_{dl} of the FGP electrodes are: 30, 42, 53, 51 mF cm^{-2}, and their corresponding ECSA are: 750, 1050, 1325, 1275 cm^2.

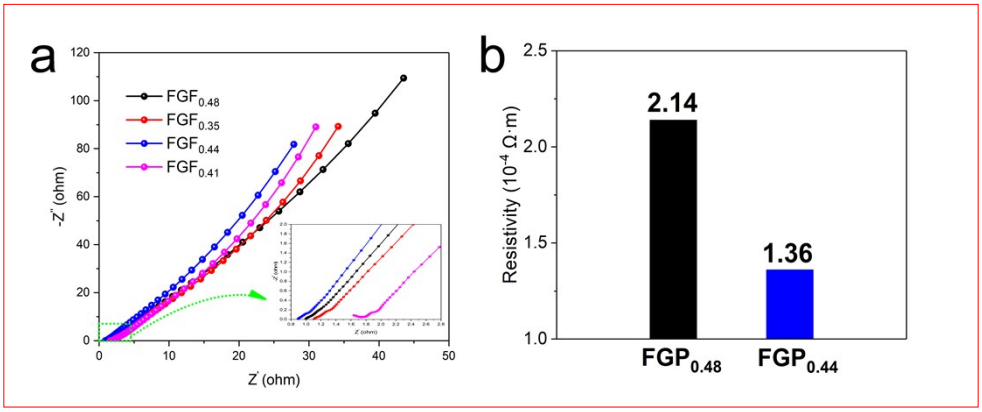

Figure S5. (a) EIS plots of $FGP_{0.48}$, $FGP_{0.35}$, $FGP_{0.44}$, and $FGP_{0.41}$ at 0.924 V (vs. RHE). Inset: the enlarged EIS plots at the high-frequency region. (b) The resistivity comparison of $FGP_{0.48}$ and $FGP_{0.44}$.

The EIS of FGP electrodes were measured to characterize their conductivity and Fig. S5a shows their Nyquist plots. Obviously, $FGP_{0.44}$ has the largest slope and the smallest X-axis intercept (the inset of Fig. S5a), showing its optimal electron transport process and conductivity.[6] The total impedance values of $FGP_{0.48,}$ $FGP_{0.35}$, $FGP_{0.44}$, and $FGP_{0.41}$ after fitting are: 1.189, 1.092, 0.943, and 2.439 Ω, respectively. The larger impedance value of $FGP_{0.41}$ may be due to the large number of functional groups adsorbed on the exfoliated graphene surface during the electrochemical process, which results in a larger contact resistance between the electrolyte and the graphene so that it shows an increased resistance value. Besides, the resistivities of the $FGP_{0.48}$ and $FGP_{0.44}$ electrodes were detected by a four-point probe measurement (Fig. S5b). The results show that the resistivity of the FGP after exfoliating decreased from 2.14×10^{-4} to 1.36×10^{-4} Ω·m, showing the increased electrical conductivity of the functionalized graphene.

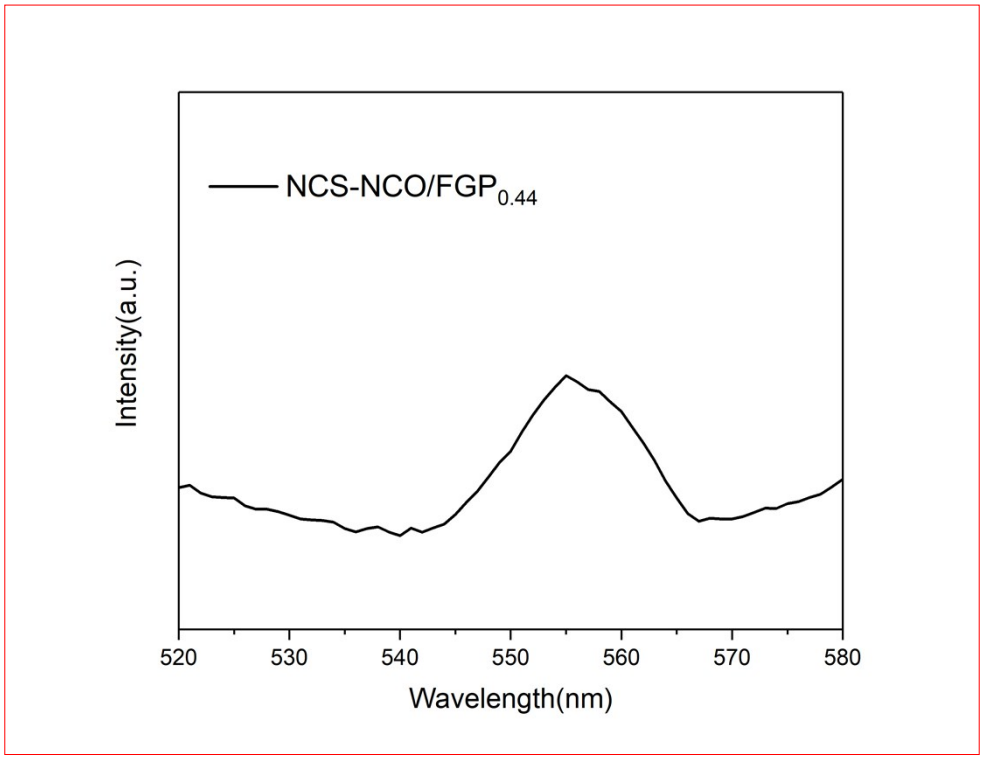

Figure S6. Photoluminescence (PL) spectra for NCS-NCO/$FGP_{0.44}$.

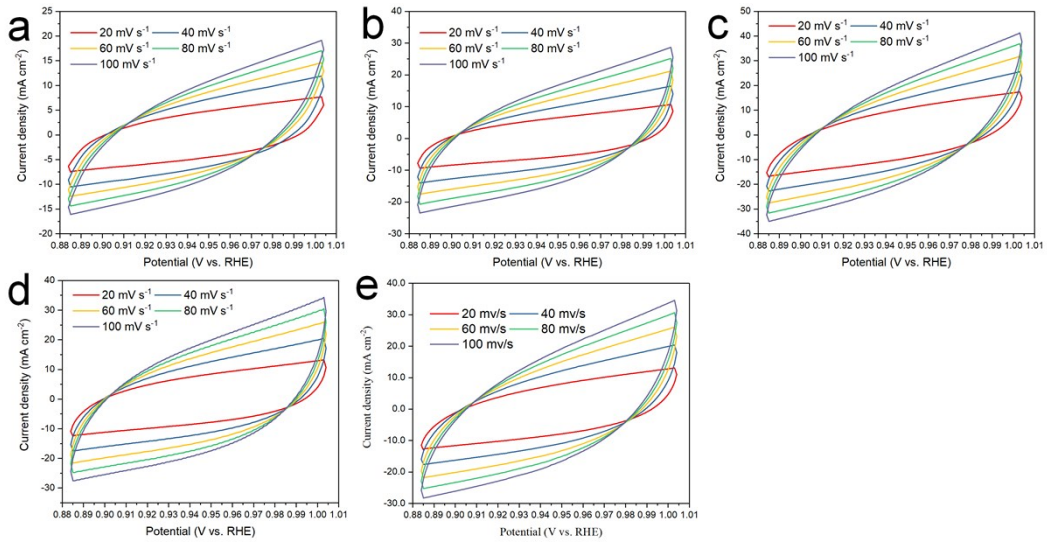

Figure S7. CV curve of NCS-NCO/FGP$_{0.48}$ (a), NCS-NCO/FGP$_{0.35}$ (b), NCS-NCO/FGP$_{0.44}$ (c), NCS-NCO/FGP$_{0.41}$ (d), and NCO/FGP$_{0.44}$ (e) under different scan rates.

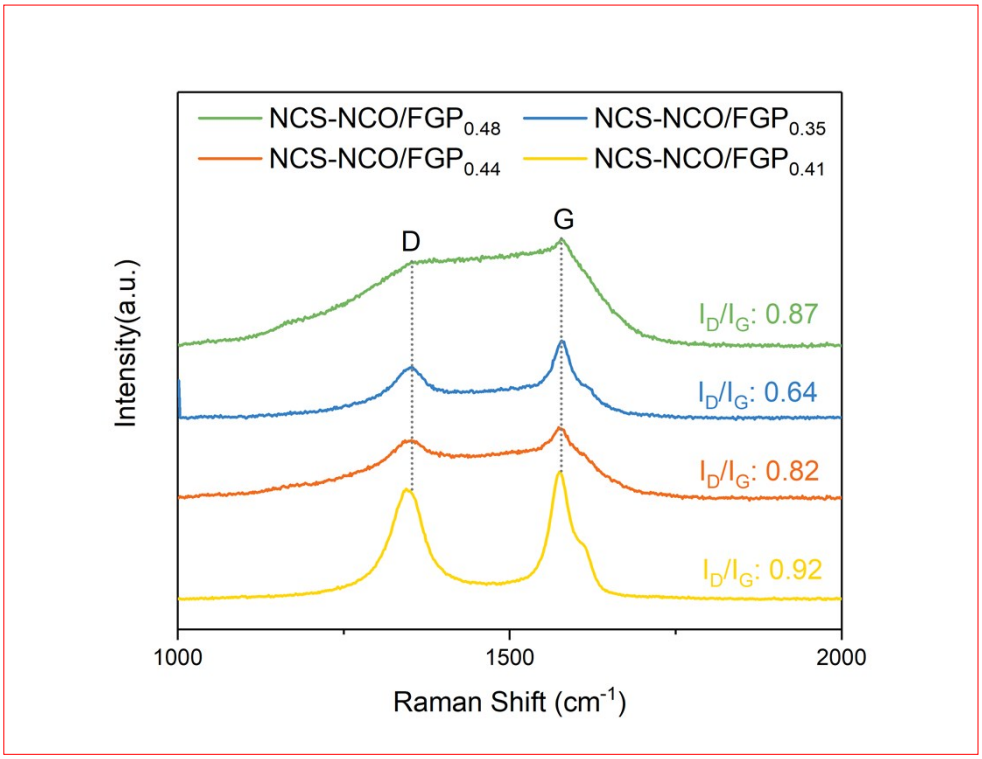

Figure S8. Raman spectra of NCS-NCO/FGP$_{0.48}$, NCS-NCO/FGP$_{0.35}$, NCS-NCO/FGP$_{0.44}$, and NCS-NCO/FGP$_{0.41}$ with their D and G peaks.

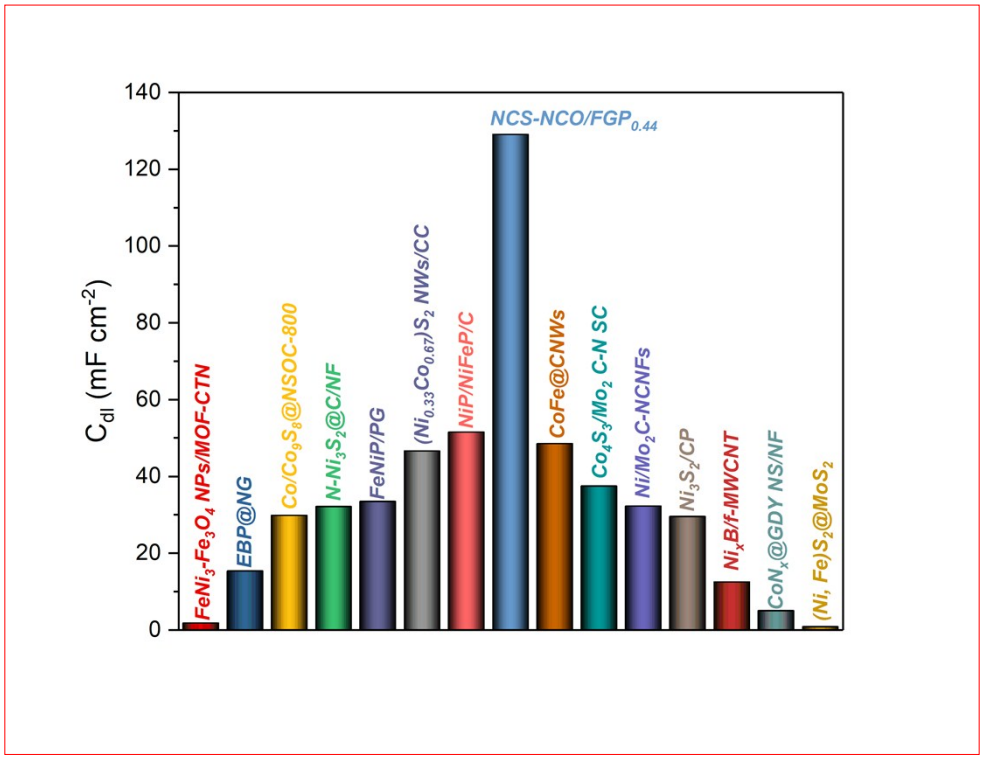

Figure S9. The comparison of C_{dl} from recent report carbon-based bifunctional electrocatalysts and NCS-NCO/FGP$_{0.44}$.

The C_{dl} of these carbon-based bifunctional electrocatalysts were performed in a 1M KOH solution. Its calculations are all derived from the CV curves without Faradaic progress. [7-20]

Table of the content

Table S1. The percentage areas of oxygen-containing functional groups in $FGP_{0.48}$, $FGP_{0.35}$, $FGP_{0.44}$, and $FGP_{0.41}$, which calculated by fitting the corresponding XPS peaks, respectively.

Table S2. The atomic content of anchored Ni and Co cations for NCS-NCO/$FGP_{0.48}$, NCS-NCO/$FGP_{0.35}$, NCS-NCO/$FGP_{0.44}$, NCS-NCO/$FGP_{0.41}$, which was calculated by ICP-OES.

Table S3. EIS data fitting results of NCS-NCO/$FGP_{0.48}$, NCS-NCO/$FGP_{0.35}$, NCS-NCO/$FGP_{0.44}$, NCS-NCO/$FGP_{0.41}$, and NCO/$FGP_{0.44}$ electrodes for OER, respectively.

Table S4. Comparison of the electrochemical performances of NCS-NCO/$FGP_{0.44}$ electrode for OER with recently reported catalysts in 1.0 M KOH.

Table S5. EIS data fitting results of NCS-NCO/$FGP_{0.48}$, NCS-NCO/$FGP_{0.35}$, NCS-NCO/$FGP_{0.44}$, NCS-NCO/$FGP_{0.41}$, and NCO/$FGP_{0.44}$ electrodes for HER.

Table S6. Comparison of the electrochemical performances of NCS-NCO/$FGP_{0.44}$ electrode for HER with recently reported catalysts in 1.0 M KOH.

Table S7. Catalyst loadings of NCS-NCO/$FGP_{0.48}$, NCS-NCO/$FGP_{0.35}$, NCS-NCO/$FGP_{0.44}$, NCS-NCO/$FGP_{0.41}$, and NCO/$FGP_{0.44}$ electrodes.

Table S8. Comparison of the electrochemical performances of NCS-NCO/$FGP_{0.44}$ electrode for overall water splitting with recently reported catalysts in 1.0 M KOH.

Table S9. Parameter settings of NCS-NCO/$FGP_{0.44}$ electrode during microwave hydrothermal synthesis.

Table S1. The percentage areas of oxygen-containing functional groups in $FGP_{0.48}$, $FGP_{0.35}$, $FGP_{0.44}$, and $FGP_{0.41}$, which calculated by fitting the corresponding XPS peaks, respectively.

Electrodes	**C-C**	**oxygen-containing functional groups**				**Area 1[a]**	**Area 2[b]**	**Percentage[c]**
		C-OH	C-O	C=O	O-C=O			
$FGP_{0.48}$	61502.34	32044.11	14845.46	-	10156.81	118548.72	57046.38	0.48
$FGP_{0.35}$	78944.59	9268.97	16531.68	4790.32	11381.39	120916.94	41972.35	0.35
$FGP_{0.44}$	65612.39	11239.78	22391.02	9781.33	8191.45	117215.97	51603.58	0.44
$FGP_{0.41}$	127433.30	27318.62	25924.30	20520.75	14584.25	215781.22	88347.92	0.41

[a] The areas of all peaks in C 1s.
[b] The areas of the peaks of oxygen-containing functional groups.
[c] The percentage areas of oxygen-containing functional groups.

Table S2. The atomic content of anchored Ni and Co cations for NCS-NCO/$FGP_{0.48}$, NCS-NCO/$FGP_{0.35}$, NCS-NCO/$FGP_{0.44}$, and NCS-NCO/$FGP_{0.41}$, which were counted by ICP-OES.

Electrodes	**The atomic content of metal cations anchored (μmol cm^{-2})**		
	Ni	Co	Sum[a]
NCS-NCO/$FGP_{0.48}$	4.29	10.53	14.82
NCS-NCO/$FGP_{0.35}$	4.17	15.49	19.66
NCS-NCO/$FGP_{0.44}$	4.36	13.37	17.73
NCS-NCO/$FGP_{0.41}$	5.06	14.51	19.57

[a] The sum atomic content of anchored metal cations.

Table S3. EIS data fitting results of NCS-NCO/$FGP_{0.48}$, NCS-NCO/$FGP_{0.35}$, NCS-NCO/$FGP_{0.44}$, NCS-NCO/$FGP_{0.41}$, and NCO/$FGP_{0.44}$ electrodes for OER, respectively.

Electrode	R_s (Ω)	R_{dl} (Ω)	R_{ct} (Ω)	R_{tot} (Ω)
NCS-NCO/$FGP_{0.48}$	1.129	1.326	4.253	6.708
NCS-NCO/$FGP_{0.35}$	1.307	1.238	4.068	6.613
NCS-NCO/$FGP_{0.44}$	**1.095**	**1.277**	**3.215**	**5.587**
NCS-NCO/$FGP_{0.41}$	1.389	1.658	4.057	7.104
NCO/$FGP_{0.44}$	1.389	0.641	4.909	6.939

Table S4. Comparison of the electrochemical performances of NCS-NCO/$FGP_{0.44}$ electrode for OER with recently reported catalysts in 1.0 M KOH.

Electrode	Substrate	j ($mA\ cm^{-2}$)	η (mV vs RHE)	Ref.
NCS-NCO/$FGP_{0.48}$	$FGP_{0.48}$	10	246	This work
NCS-NCO/$FGP_{0.35}$	$FGP_{0.35}$	10	291	
NCS-NCO/$FGP_{0.44}$	**$FGP_{0.44}$**	**10**	**117**	
NCS-NCO/$FGP_{0.41}$	$FGP_{0.41}$	10	199	
NCO/$FGP_{0.44}$	$FGP_{0.44}$	10	304	
RuO_2/$FGP_{0.44}$	$FGP_{0.44}$	10	320	
CoS_2−C@MoS_2	-	10	391	[21]
Ni_3S_2	-	10	295	[17]
Ni_3S_2	NF	10	296	[22]
$CoMoS_4$/Ni_3S_2	NF	10	200	[23]
$CoS_xSe_{2(1-x)}$	CC	10	285	[24]
CoN_x@GDY	GDY[a]-modified NF	10	260	[19]
MoS_2/NiCoS heterostructure	-	10	290	[25]
(Ni, Fe) S_2@MoS_2 heterostructrues	CFP[b]	10	270	[20]
Pt–αFe_2O_3	NF	50	304	[26]
Ru/$Cu_{2+1}O$	CuF[c]	10	210	[27]

[a] Graphdiyne.
[b] Carbon fiber paper.
[c] Cu foam

Table S5. EIS data fitting results of NCS-NCO/$FGP_{0.48}$, NCS-NCO/$FGP_{0.35}$, NCS-NCO/$FGP_{0.44}$, NCS-NCO/$FGP_{0.41}$, and NCO/$FGP_{0.44}$ electrodes for HER.

Electrode	**R_s (Ω)**	**R_{dl1} (Ω)**	**R_{dl2} (Ω)**	**R_{ct} (Ω)**	**R_{tot} (Ω)**
NCS-NCO/$FGP_{0.48}$	1.027	0.556	1.390	5.100	8.073
NCS-NCO/$FGP_{0.35}$	1.413	0.324	1.046	4.400	7.183
NCS-NCO/$FGP_{0.44}$	**1.075**	**0.204**	**0.757**	**3.335**	**5.371**
NCS-NCO/$FGP_{0.41}$	0.883	0.374	1.293	4.330	6.880
NCO/$FGP_{0.44}$	1.469	0.341	1.289	4.882	7.981

Table S6. Comparison of the electrochemical performances of NCS-NCO/$FGP_{0.44}$ electrode for HER with recently reported catalysts in 1.0 M KOH.

Catalyst	Substrate	j (mA cm^{-2})	η (mV vs. RHE)	Ref.
NCS-NCO/$FGP_{0.48}$	$FGP_{0.48}$	10	-219	This work
NCS-NCO/$FGP_{0.35}$	$FGP_{0.35}$	10	-172	
NCS-NCO/$FGP_{0.44}$	**$FGP_{0.44}$**	**10**	**-145**	
NCS-NCO/$FGP_{0.41}$	$FGP_{0.41}$	10	-199	
NCO/$FGP_{0.44}$	$FGP_{0.44}$	10	-235	
Pt/C/$FGP_{0.44}$	$FGP_{0.44}$	10	-30	
CoS_2–C@MoS_2	-	10	-173	[21]
Ni_3S_2	-	10	-112	[17]
Ni_3S_2	NF	10	-189	[22]
$CoMoS_4/Ni_3S_2$	NF	10	-76	[23]
$CoS_xSe_{2(1-x)}$	CC	10	-225	[24]
CoN_x@GDY	GDY-modified NF	10	-70	[19]
MoS_2/NiCoS heterostructure	-	10	189	[25]
(Ni, Fe) S_2@MoS_2 heterostructrues	CFP	10	-130	[20]
Pt–αFe_2O_3	NF	10	-90	[26]
Ru/$Cu_{2+1}O$	CuF	10	-32	[27]

Table S7. Catalyst loading of NCS-NCO/$FGP_{0.48}$, NCS-NCO/$FGP_{0.35}$, NCS-NCO/$FGP_{0.44}$, NCS-NCO/$FGP_{0.41}$, and NCO/$FGP_{0.44}$ electrodes.

Electrode	Mass of catalyst (mg cm^2)		Catalyst loading (mg cm^2)
	m_0[a]	m_1[b]	Δm[c]
NCS-NCO/$FGP_{0.48}$	148.6	134.1	14.5
NCS-NCO/$FGP_{0.35}$	128.5	113.1	15.4
NCS-NCO/$FGP_{0.44}$	139.3	122.6	16.7
NCS-NCO/$FGP_{0.41}$	136.5	119.9	16.6
NCO/$FGP_{0.44}$	129.3	119.1	10.2

[a] The mass of the catalysts before acid treatment
[b] The mass of the catalysts after acid treatment
[c] Catalyst loading: $\Delta m = m_0 - m_1$

Table S8. Comparison of the electrochemical performances of NCS-NCO/$FGP_{0.44}$ electrode for overall water splitting with recently reported catalysts in 1.0 M KOH.

Catalyst	Substrate	j (mA cm^{-2})	η (mV vs RHE)	Ref.
NCS-NCO/$FGP_{0.48}$	$FGP_{0.48}$	10	1.580	
NCS-NCO/$FGP_{0.35}$	$FGP_{0.35}$	10	1.544	This work
NCS-NCO/$FGP_{0.44}$	**$FGP_{0.44}$**	**10**	**1.481**	
NCS-NCO/$FGP_{0.41}$	$FGP_{0.41}$	10	1.596	
NCO/$FGP_{0.44}$	$FGP_{0.44}$	10	1.636	
RuO_2/$FGP_{0.44}$ Pt/C/$FGP_{0.44}$	$FGP_{0.44}$	10	1.583	
Ni_3S_2	-	10	1.63	[17]
Ni_3S_2	NF	10	~1.55	[22]
$CoMoS_4/Ni_3S_2$	NF	10	1.568	[23]
$CoS_xSe_{2(1-x)}$	CC	10	1.74	[24]
CoN_x@GDY	GDY-modified NF	10	1.48	[19]
MoS_2/NiCoS heterostructure	NF	10	1.50	[25]
(Ni, Fe) S_2@MoS_2 heterostructrues	CFP	10	1.56	[20]
Pt–αFe_2O_3	NF	10	1.51	[26]
Ru/$Cu_{2+1}O$	CuF	10	1.53	[27]

Table S9. Parameter settings of NCS-NCO/$FGP_{0.44}$ electrode during microwave hydrothermal synthesis.

Experimental stage	Temperature (°C)	Operating time (min)	Power (W)
1	30	0	600
2	120	10	600
3	120	5	600
4	160	10	600
5	160	5	600
6	200	12	600
7	200	45	600

References

1 Y. Zhu, L. Zhang, B. Zhao, H. Chen, X. Liu, R. Zhao, X. Wang, J. Liu, Y. Chen and M. Liu, *Adv. Funct. Mater.*, 2019, **29**, 1901783.
2 B. Liu, J. Cheng, H.-Q. Peng, D. Chen, X. Cui, D. Shen, K. Zhang, T. Jiao, M. Li, C.-S. Lee and W. Zhang, *J. Mater. Chem. A*, 2019, **7**, 775-782.
3 Z. Li, Y. Zhang, Y. Feng, C.-Q. Cheng, K.-W. Qiu, C.-K. Dong, H. Liu and X.-W. Du, *Adv. Funct. Mater.*, 2019, **29**, 1903444.
4 M. Seredych, D. Hulicova-Jurcakova, G. Q. Lu and T. J. Bandosz, *Carbon*, 2008, **46**, 1475-1488.
5 W. Yang, J. Tian, L. Hou, B. Deng, S. Wang, R. Li, F. Yang and Y. Li, *ChemSusChem*, 2019, **12**, 4662-4670.
6 Q. Dong, Y. Zhang, Z. Dai, P. Wang, M. Zhao, J. Shao, W. Huang and X. Dong, *Nano Res.*, 2018, **11**, 1389-1398.
7 K. Srinivas, Y. Lu, Y. Chen, W. Zhang and D. Yang, *ACS Sustainable Chem. Eng.*, 2020, **8**, 3820-3831.
8 Z. Yuan, J. Li, M. Yang, Z. Fang, J. Jian, D. Yu, X. Chen and L. Dai, *J. Am. Chem. Soc.*, 2019, **141**, 4972-4979.
9 J. Du, R. Wang, Y.-R. Lv, Y.-L. Wei and S.-Q. Zang, *Chemical Communications*, 2019, **55**, 3203-3206.
10 Q. Hao, S. Li, H. Liu, J. Mao, Y. Li, C. Liu, J. Zhang and C. Tang, *Catal. Sci. Technol.*, 2019, **9**, 3099-3108.
11 F. Bu, W. Chen, M. F. Aly Aboud, I. Shakir, J. Gu and Y. Xu, *J. Mater. Chem. A*, 2019, **7**, 14526-14535.
12 Q. Zhang, C. Ye, X. L. Li, Y. H. Deng, B. X. Tao, W. Xiao, L. J. Li, N. B. Li and H. Q. Luo, *ACS Appl. Mater. Interfaces*, 2018, **10**, 27723-27733.
13 B. Weng, X. Wang, C. R. Grice, F. Xu and Y. Yan, *J. Mater. Chem. A*, 2019, **7**, 7168-7178.
14 X. Wang, B. Zheng, D. Yang, B. Sun, W. Zhang and Y. Chen, *Energy Technol.*, 2019, **0**.
15 Y. Liu, X. Luo, C. Zhou, S. Du, D. Zhen, B. Chen, J. Li, Q. Wu, Y. Iru and D. Chen, *Appl. Catal. B Environ.*, 2020, **260**, 118197.
16 M. Li, Y. Zhu, H. Wang, C. Wang, N. Pinna and X. Lu, *Adv. Energy Mater.*, 2019, **9**, 1803185.
17 X. Zheng, X. Han, Y. Zhang, J. Wang, C. Zhong, Y. Deng and W. Hu, *Nanoscale*, 2019, **11**, 5646-5654.
18 X. Chen, Z. Yu, L. Wei, Z. Zhou, S. Zhai, J. Chen, Y. Wang, Q. Huang, H. E. Karahan, X. Liao and Y. Chen, *J. Mater. Chem. A*, 2019, **7**, 764-774.
19 Y. Fang, Y. Xue, L. Hui, H. Yu, Y. Liu, C. Xing, F. Lu, F. He, H. Liu and Y. Li, *Nano Energy*, 2019, **59**, 591-597.
20 Y. Liu, S. Jiang, S. Li, L. Zhou, Z. Li, J. Li and M. Shao, *Appl. Catal. B Environ.*, 2019, **247**, 107-114.
21 Y. Zhu, L. Song, N. Song, M. Li, C. Wang and X. Lu, *ACS Sustainable Chem. Eng.*, 2019, **7**, 2899-2905.
22 L. Li, C. Sun, B. Shang, Q. Li, J. Lei, N. Li and F. Pan, *J. Mater. Chem. A*, 2019, **7**, 18003-18011.
23 P. Hu, Z. Jia, H. Che, W. Zhou, N. Liu, F. Li and J. Wang, *J. Power Sources*, 2019, **416**, 95-103.
24 Y. Zhang, Y. Qiu, X. Ji, T. Ma, Z. Ma and P. A. Hu, *ChemSusChem*, 2019, **12**, 3792-3800.
25 C. Qin, A. Fan, X. Zhang, S. Wang, X. Yuan and X. Dai, *J. Mater. Chem. A*, 2019, **7**, 27594-27602.
26 B. Ye, L. Huang, Y. Hou, R. Jiang, L. Sun, Z. Yu, B. Zhang, Y. Huang and Y. Zhang, *J. Mater. Chem. A*, 2019, **7**, 11379-11386.
27 J. Gao, L. Yang, D. Wang and D. Cao, *Chem. Eur. J.*, 2019, **n/a**.